Vietnam Journal of Mechanics, Vol. 46, No. 3 (2024), pp. 217 – 228
DOI: https://doi.org/10.15625/0866-7136/21007

A STAGGERED LOCAL DAMAGE MODEL FOR FRACTURE ANALYSIS IN BI-MATERIAL STRUCTURES

Manh Van Pham[1,2], **Minh Ngoc Nguyen**[1,3], **Tinh Quoc Bui**[1,3]
[1]*Duy Tan Research Institute for Computational Engineering (DTRICE), Duy Tan University, Ho Chi Minh City 70000, Vietnam*
[2]*University of Architecture Ho Chi Minh City, Ho Chi Minh City 70000, Vietnam*
[3]*Faculty of Civil Engineering, Duy Tan University, Da Nang City 55000, Vietnam*
*E-mail: manh.phamvan@uah.edu.vn

Received: 29 February 2024 / Revised: 12 April 2024 / Accepted: 18 June 2024
Published online: 09 July 2024

Abstract. This article is devoted to extension of the recently developed enhanced local damage model for failure prediction in bi-material structures. Compared to non-local models, the enhanced local model offers lower computational cost while the inherent mesh-dependency issue is treated. By defining equivalent strain based on the bi-energy norm concept and Mazars's criterion, which considers both tensile and compressive strain components, the model aligns with the behavior of quasi-brittle materials. The state of material point is indicated by a damage parameter, ranging from 0 to 1, to represent the evolution from being fully intact to complete failure. An efficient staggered scheme is introduced, in which the equilibrium equation and the update of damage parameter are decoupled. The proposed model is validated with a series of three-point bending experimental tests on PMMA/Al6061 specimens reported by Lee and Krishnaswamy (2000). Good agreement is observed between the proposed model and experimental data, as well as numerical results from other authors, in crack path prediction.

Keywords: enhanced local damage, bi-material structures, fracture analysis, staggered scheme.

1. INTRODUCTION

Due to the wide application of brittle/quasi-brittle materials in various engineering fields, the study on integrity of structures made from such materials is of importance and attracts much attention. In the context of continuum damage model, the state of material is represented by a continuous field with values from 0 to 1, capturing the evolution from intactness to complete failure. There are two primary categories of damage model:

local model and non-local/gradient-enhanced model. Although the local model [1, 2] is simple, it is suffered from inherent issue of mesh-dependency. In order to overcome such difficulty, the non-local/gradient-enhanced damage model was introduced at the expense of additional computational effort [3, 4]. The evolution of damage parameter is usually driven by an internal variable reflecting the loading history, which is usually calculated from strain components and thus it is called equivalent strain. Because stress and strain are related, stress-based damage models also exist, see [4] for example. For non-local/gradient-enhanced damage, the non-local equivalent strain is further calculated via an integral (non-local model), or via partial differential equation (gradient-enhanced model). Recently, Kurumatani et al. [5] improved the local model by incorporating the fracture energy and the element characteristic length into the calculation of damage parameter, which helped to mitigate the mesh-dependency issue. Pham et al. further extended the approach in two aspects: i) introduction of a new equivalent strain [6], which is shown to be more suitable than the one based on modified von Mises criterion used by [5] in mixed-mode problems; and ii) consideration of damage induced by both mechanical and thermal loads [7].

However, while in the available literature, while there is plenty of works on damage modeling which focus on homogeneous materials, the amount of publications on failure prediction in heterogeneous materials is still limited. An experimental study by Lee and Krishnaswamy [8] for three-point bending of pre-notched PMMA/Al6061 specimens revealed different crack paths corresponding to different boundary conditions. The experiment was later used for validation of several numerical models, including a model based on the FRANC2D/3D software [8], an S-version finite element approach [9], and a recent localizing gradient damage model [10].

The objective of this paper is extension of the enhanced local damage model by Pham et al. [6,7] for failure analysis of structures with heterogeneous materials, particularly the bi-material structures. Furthermore, an efficient staggered scheme on the basis of finite element method is proposed to solve the non-linear problems. The proposed approach is validated by comparison with the experimental data reported in [8], as well as results from other numerical models.

2. FORMULATION OF LOCAL DAMAGE MODEL

2.1. Basic equations

Given a domain Ω with boundary $\partial\Omega$, the strong form equilibrium equation under quasi-static boundary conditions is written as

$$\nabla \cdot \boldsymbol{\sigma} + \mathbf{b} = 0, \tag{1}$$

where $\mathbf{b}$ denotes the body force and $\boldsymbol{\sigma}$ is the stress tensor. In order to account for elastic-damage behavior, the stress-strain relation is expanded beyond Hooke's law by

$$\boldsymbol{\sigma} = (1-d)\,\mathbf{C}\colon \boldsymbol{\varepsilon}, \tag{2}$$

in which $d \in [0,1]$ is a scalar parameter characterizing the state of material from being intact ($d = 0$) to complete failure ($d = 1$), and $\mathbf{C}$ is the elastic tensor. Under the assumption of small deformations, the components of the strain tensor $\boldsymbol{\varepsilon}$ can be determined from the displacements $\mathbf{u} = [u_1, u_2, u_3]^T$ by applying the following equations

$$\varepsilon_{ij} = \frac{1}{2}\left(\frac{\partial u_i}{\partial x_j} + \frac{\partial u_j}{\partial x_j}\right) \text{ with } i,j = 1,2,3. \tag{3}$$

For quasi-brittle material, the evolution of damage is usually quantified by

$$d(\kappa) = \begin{cases} 0, & \text{if } \kappa \leq \kappa_0, \\ 1 - \dfrac{\kappa}{\kappa_0}\left[1 - \alpha + \alpha e^{-\beta(\kappa-\kappa_0)}\right], & \text{otherwise.} \end{cases} \tag{4}$$

Here E is the Young's elastic modulus. κ_0 is the strain value corresponding to the load capacity f_t in uniaxial tensile experiment, an can be calculated as

$$\kappa_0 = \frac{f_t}{E}. \tag{5}$$

Since healing is not considered, the irreversibility of damage has to be enforced. The internal variable κ must be non-decreasing and is determined by the maximum value of equivalent strain, $\tilde{\varepsilon}$, in the deformation history

$$\begin{cases} \kappa \geq 0, \\ \kappa = \max(\tilde{\varepsilon})\,. \end{cases} \tag{6}$$

Various forms of equivalent strain have been proposed in the literature for different purposes, based on different criterion, for e.g., the modified von-Mises criterion [11], the Mazars's criterion [12] and the bi-energy norm concept [13]. In Eq. (5), the shape parameters α and β characterize the softening curve of the stress-strain relation (see Fig. 1) and can be determined by fitting experimental data. For simplicity, $\alpha = 1$ is chosen in this study.

The local continuum damage model, as presented above, has been found to be susceptible to mesh dependency. As an attempt to overcome such drawback, Kurumatani et al. [5] proposed that the β parameter, which represents the material toughness, can be considered as a coefficient based on the 1D relationship between the cohesive force and the crack opening displacement. It is observed that the fracture energy G_f, which is typically obtained from a uniaxial tensile experiment, includes both the elastic strain

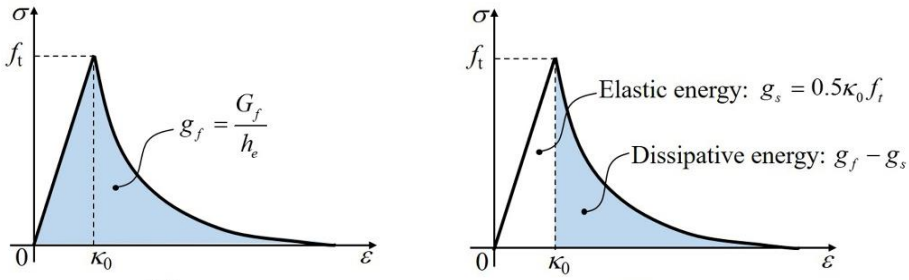

Fig. 1. Fracture energy unit length: (a) the usual value given by uniaxial tensile experiment and (b) the proposal for subtraction of elastic energy from fracture energy [6]

energy and the dissipative energy due to crack opening [14], as shown in Fig. 1. However, from a numerical computation perspective, it is critical to subtract the elastic strain energy ($g_s = 0.5\kappa_0 f_t$) from G_f. Therefore, parameter β can be formulated as follows [6]

$$\beta = \frac{E\kappa_0 h_e}{G_f - 0.5\kappa_0 f_t h_e}, \tag{7}$$

where h_e is the element characteristic length. Particularly for quadrilateral element, this quantity can be calculated as $h_e = \sqrt{A_e}$ (see [5]), with A_e being the area of the element. In Eq. (8), the value of β varies from element to element.

On the basis of the bi-energy concept [13], the equivalent strain is decomposed to tension and compression parts. Here, determination of the tensile and compressive strain components is inspired by the Mazars model [12], which was developed based on experiments. Then, the so-called "enhanced bi-energy norm equivalent strain" is defined as follows:

$$\widetilde{\varepsilon} = \frac{kr\widetilde{\varepsilon}_t + (1-r)\,\widetilde{\varepsilon}_c}{\lambda\,(k+1)}, \tag{8}$$

where k is a ratio between compressive strength, f_c, and tensile strength, f_t, i.e., $k = f_c / f_t$, which usually falls within the range k = 5–10 depending on the particular material. λ is an empirical coefficient and, as reported in [13], can be taken from 0.7 to 1.0 to fit experimental data. Here $\widetilde{\varepsilon}_c$ and $\widetilde{\varepsilon}_t$ are calculated by [12]

$$\widetilde{\varepsilon}_c = \frac{I_1}{5\,(1-2\nu)} + \frac{6\sqrt{3J_2}}{5\,(1+\nu)}, \quad \widetilde{\varepsilon}_t = \frac{I_1}{2\,(1-2\nu)} + \frac{\sqrt{3J_2}}{2\,(1+\nu)}, \tag{9}$$

in which ν is the Poisson's ratio; I_1 is the first invariant of the strain tensor; and J_2 is the second invariant of the deviatoric strain tensor.

Parameter r in Eq. (9) is the triaxial factor [6] that indicates the stress state, in which the values vary from 0 (compressive domain) to 1 (tensile domain):

$$r = \frac{\sum \langle \overline{\sigma}_i \rangle}{\sum |\overline{\sigma}_i|}, \tag{10}$$

with $\overline{\sigma}_i$ being the principal value of the "effective stress tensor" $\overline{\boldsymbol{\sigma}} = \mathbf{C} : \boldsymbol{\varepsilon}$, i.e., the stress values without consideration of damage. The Macaulay bracket $\langle \overline{\sigma}_i \rangle$ returns $\overline{\sigma}_i$ if it is positive, and returns 0 otherwise.

2.2. Formulation equations for the damage problems

From (3), the weak form balance equation for the problem is written as follows

$$\int_{\Omega} \mathbf{B}^T (1-d)\, \mathbf{C}\boldsymbol{\varepsilon} \mathrm{d}\Omega - \int_{\Gamma_t} \mathbf{N}^T \bar{\mathbf{t}} \mathrm{d}\Gamma - \int_{\Omega} \mathbf{N}^T \mathbf{b} \mathrm{d}\Omega = 0, \tag{11}$$

where $\mathbf{N}$ and $\mathbf{B}$ are the matrices that store the shape functions and their spatial derivatives; $\bar{\mathbf{t}}$ is the prescribed traction on surface and $\mathbf{b}$ is the body force.

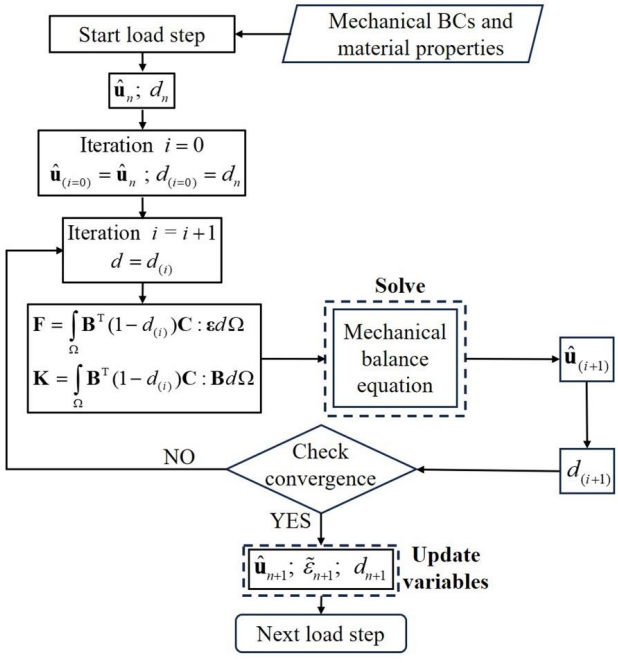

Fig. 2. A flow chart for the staggered scheme employed of one load step to solve damage problems

Here, we propose a staggered scheme such that the mechanical equilibrium (Eq. (11)) and the damage evolution (Eq. (5)) are decoupled. A flow chart is given in Fig. 2. At load

step $n+1$, all values at load step n are known and can be set as initial values for iterative procedure: $\hat{\mathbf{u}}_{(i=0)} = \hat{\mathbf{u}}_n$, $d_{(i=0)} = d_n$. It is worth noting that the damage values are stored at integration points, whereas the displacement values are stored at nodes. At iteration $i+1$, Eq. (11) is solved to find the new displacement field $\hat{\mathbf{u}}_{i+1}$, with the assumption $d = d_i$. The damage field d_{i+1} is updated using displacement field $\hat{\mathbf{u}}_{i+1}$. The iterative process continues until the change of displacement is below a specified tolerance. The change in displacement between two consecutive iterations is calculated as $du = norm\,(\hat{\mathbf{u}}_{i+1} - \hat{\mathbf{u}}_i)$. In which, the pre-selected allowable tolerance is $TOL = 10^{-3}$. Once this condition is fulfilled, the variables are saved, and the algorithm progresses to the subsequent load step. This staggered scheme offers the advantage of simpler implementation, although it requires smaller increments to ensure accurate outcomes. Comparable approaches can be found in the literature [7, 15].

3. NUMERICAL RESULTS AND DISCUSSION

In this section, we examine a three-point bending beam with bi-material specimens composed of PMMA and aluminum alloy Al6061. In this problem, the interface between two materials is assumed to be perfectly bonded. These specimens have an initial crack, and is loaded on top edge, as described in [8]. The beam sample has a thickness of 9 mm, and the material properties are given in Table 1. Three different cases with varying boundary conditions are considered, and the initial quadrilateral element mesh is illustrated in Fig. 3. In Case (1), the crack length is 30 mm, being located at the middle of the bottom edge. A support that restrains displacement vertically and horizontally is placed at the lower left corner, while a roller which hinders only vertical displacement is placed at the lower right corner. Case (2) is similar to Case (1) in terms of the initial crack and position of prescribed displacement, but with different location of the support. In Case (3), the initial crack is longer, with a length of 70 mm, and is not aligned with the loaded position. The support is placed at a distance of 50 mm from the lower left corner. For both Case (1) and Case (2), the same mesh of 4643 quadrilateral elements are employed, while another mesh is used for Case (3) with 5505 quadrilateral elements in total. In this problem, the staggered scheme is applied to all cases with 1000 uniform loading steps corresponding to a total displacement of $\overline{u} = 0.06$ mm. So, the increment size for prescribed displacement for each loading step is $d\overline{u} = \overline{u}/1000 = 6 \times 10^{-5}$ mm. The accuracy

Table 1. Material properties used for the pre-notched PMMA/Al6061 specimens (see [8, 10])

Material	E (MPa)	ν	f_t (MPa)	G_f (N/mm)	k	κ_0
PMMA	3240	0.35	0.972	0.0039	5	3×10^{-4}
Al6061	69000	0.3	124.2	0.4968	10	18×10^{-4}

of this scheme always requires a large number of loading steps. With 1000 step loads and the increment size of displacement $d\bar{u} = 6 \times 10^{-5}$ mm , we observed that the convergence of the problem occurs faster in each iteration. This is demonstrated by the results below. It is noted that all three cases are mixed-mode problems due to the existence of heterogeneous materials.

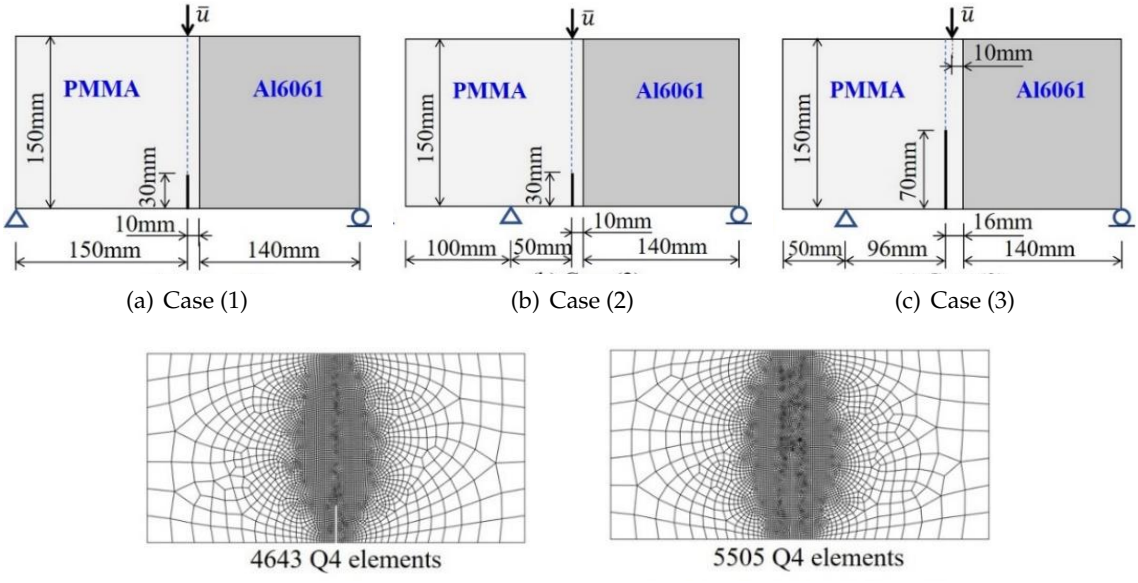

(a) Case (1) (b) Case (2) (c) Case (3)

(d) Initial mesh for Case (1), Case (2) (e) Initial mesh for Case (3)

Fig. 3. Boundary conditions, geometry, and initial mesh for PMMA/Al6061 bi-material beam

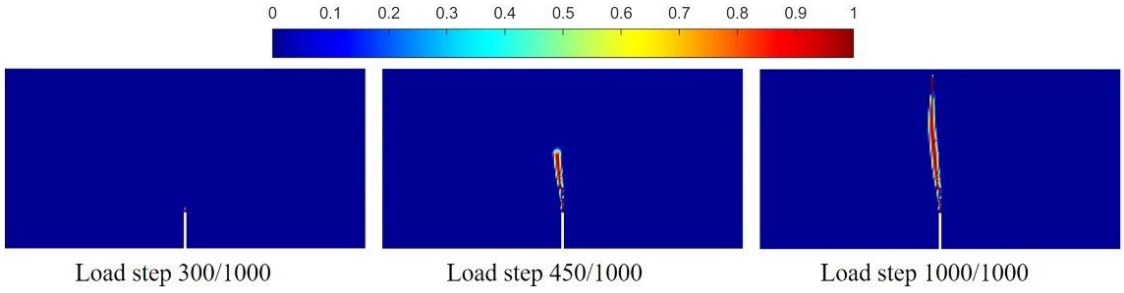

Fig. 4. Numerical prediction of propagation of damage zone for Case (1) by the developed damage model through load steps

For Case (1), the progression of the damage zone through the loading steps are shown in Fig. 4. The obtained crack path is in good agreement with both experimental and numerical results by Lee and Krishnaswamy [8], the S-version finite element method

(S-FEM) by Kikuchi et al. [9], and the localizing gradient damage model by Rajput et al. [10], as shown in Fig. 5. The crack tends to move away from the material interface. For Case (2) and Case (3), the damage progression is depicted in Fig. 6 and Fig. 8, respectively. Furthermore, Fig. 7 and Fig. 9 present a comparison between the obtained crack paths and reference results, which exhibit good agreement. In Case (2), the crack tends to move along the material interface, while in Case (3), the crack nearly moves straight upward.

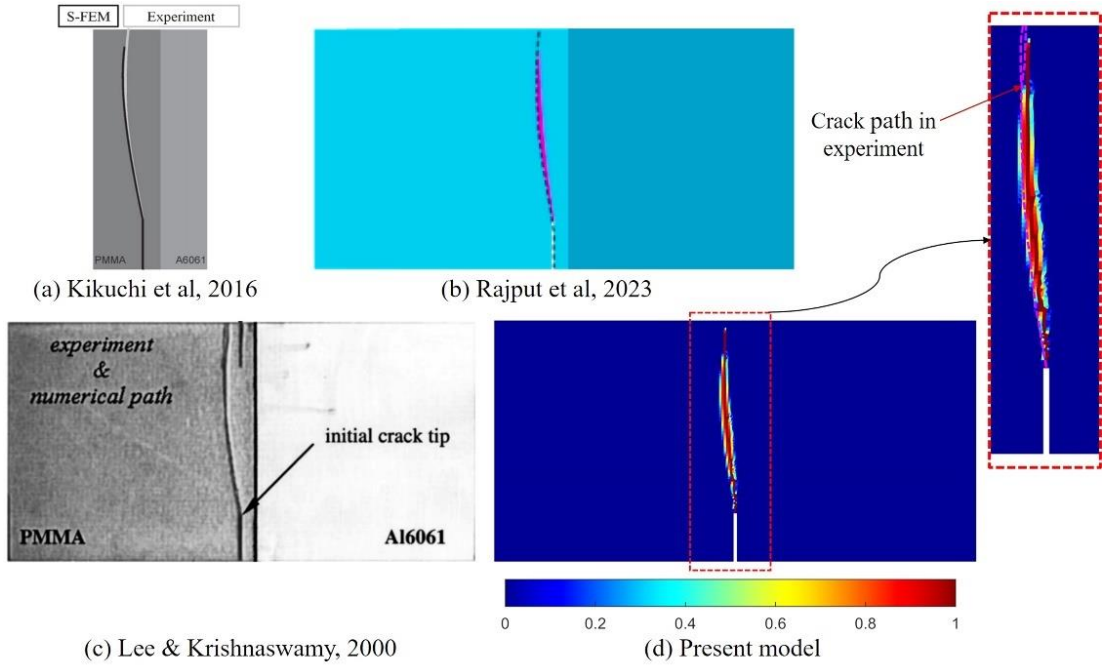

Fig. 5. Comparison on damage zone/crack path predicted by various numerical models and experiment with Case (1)

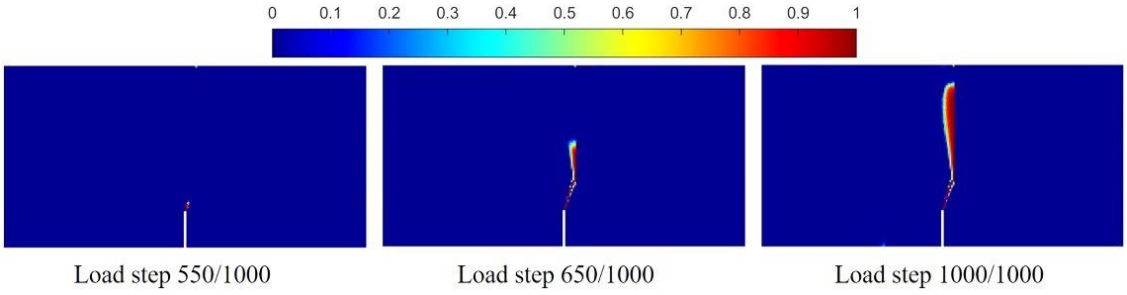

Fig. 6. Numerical prediction of propagation of damage zone for Case (2) by the developed damage model through load steps

The load-displacement responses for all three cases, which were not found in the references [8–10], are depicted in Fig. 10. In Cases (1) and (3), where the damage zone is completely within the part of PMMA, the shape of the load-displacement curves resembles the typical pattern observed in quasi-brittle materials. On the other hand, in Case (2), where the damage occur mostly along the interface, the curve exhibits the pattern usually observed in brittle materials.

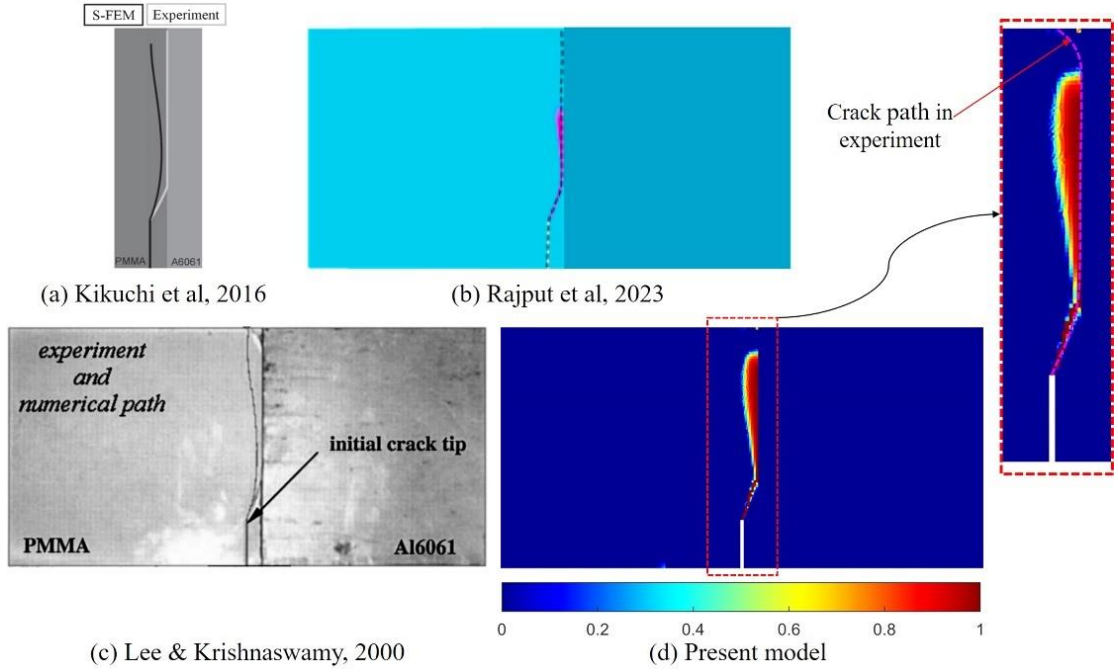

Fig. 7. Comparison on damage zone/crack path predicted by various numerical models and experiment with Case (2)

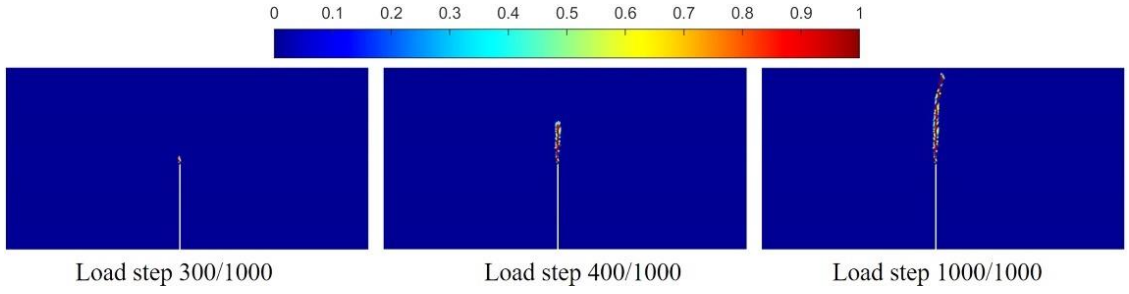

Fig. 8. Numerical prediction of propagation of damage zone for Case (3) by the developed damage model through load steps

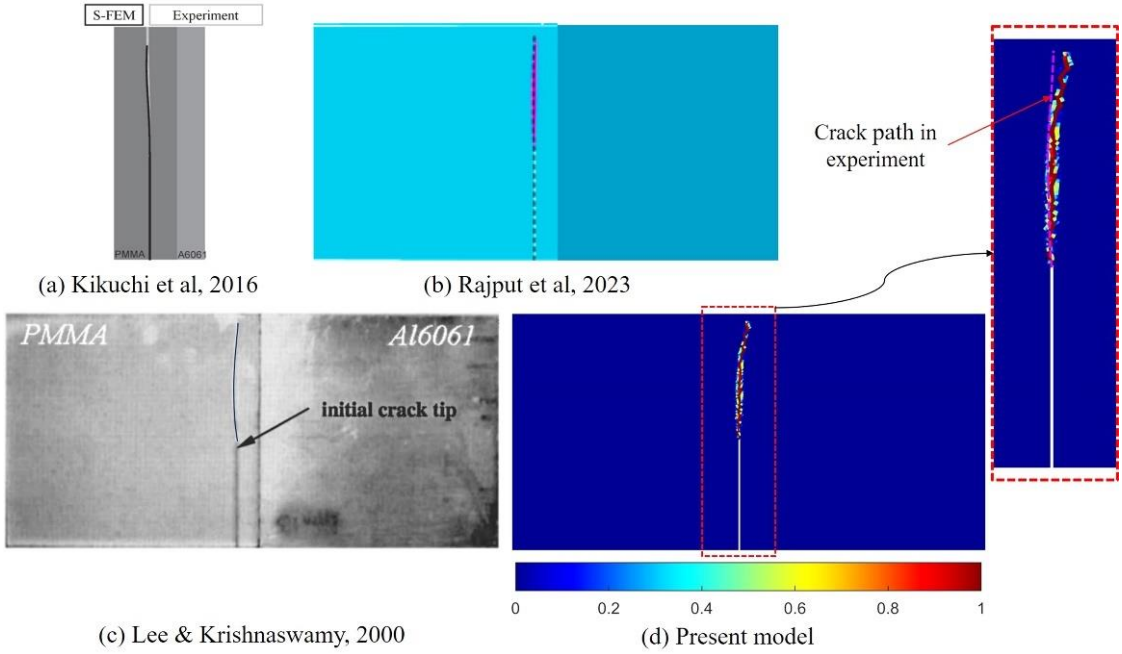

Fig. 9. Comparison on damage zone/crack path predicted by various numerical models and experiment with Case (3)

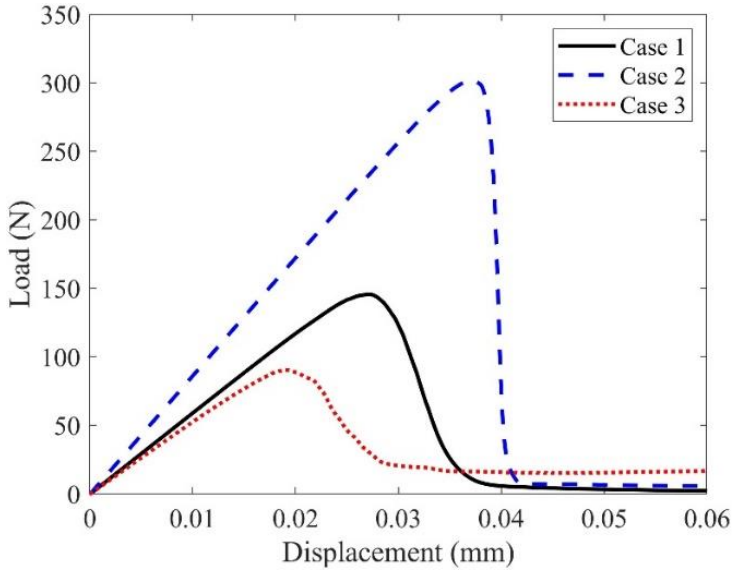

Fig. 10. Results of load - displacement response in three cases

4. CONCLUSIONS

The enhanced local damage model in previous works [6,7] for structures with homogeneous quasi-brittle materials has been successfully extended to bi-material structures. An efficient staggered scheme is introduced, which help to simplify the computational procedure. Comparison with experimental data and numerical results from other authors for the PMMA/Al6061 specimens exhibits that the proposed model is able to predict crack growth and propagation.

The obtained results are preliminary for further investigation of the performance of the proposed approach for structures with heterogeneous structures. In fact, quasi-static loading is currently assumed. The ability of the model also needs further quantitative verification.

DECLARATION OF COMPETING INTEREST

The authors declare that they have no known competing financial interests or personal relationships that could have appeared to influence the work reported in this paper.

FUNDING

This research received no specific grant from any funding agency in the public, commercial, or not-for-profit sectors.

REFERENCES

[1] L. M. Kachanov and D. Krajcinovic. Introduction to continuum damage mechanics. *Journal of Applied Mechanics*, **54**, (1987), pp. 481–481. https://doi.org/10.1115/1.3173053.

[2] J. Lemaitre and R. Desmorat. *Engineering damage mechanics: ductile, creep, fatigue and brittle failures*. Springer Science & Business Media, (2006).

[3] M. Jirásek and B. Patzák. Consistent tangent stiffness for nonlocal damage models. *Computers & Structures*, **80**, (2002), pp. 1279–1293. https://doi.org/10.1016/s0045-7949(02)00078-0.

[4] C. Giry, F. Dufour, and J. Mazars. Stress-based nonlocal damage model. *International Journal of Solids and Structures*, **48**, (2011), pp. 3431–3443. https://doi.org/10.1016/j.ijsolstr.2011.08.012.

[5] M. Kurumatani, K. Terada, J. Kato, T. Kyoya, and K. Kashiyama. An isotropic damage model based on fracture mechanics for concrete. *Engineering Fracture Mechanics*, **155**, (2016), pp. 49–66. https://doi.org/10.1016/j.engfracmech.2016.01.020.

[6] M. V. Pham, M. N. Nguyen, and T. Q. Bui. Numerical simulation of localized quasi-brittle fracture with an enhanced bi-energy norm based equivalent strain. *Engineering Fracture Mechanics*, **288**, (2023), 109340. https://doi.org/10.1016/j.engfracmech.2023.109340.

[7] M. V. Pham, M. N. Nguyen, and T. Q. Bui. A novel thermo-mechanical local damage model for quasi-brittle fracture analysis. *Theoretical and Applied Fracture Mechanics*, **130**, (2024), 104329. https://doi.org/10.1016/j.tafmec.2024.104329.

[8] H. Lee and S. Krishnaswamy. Quasi-static propagation of subinterfacial cracks. *Journal of Applied Mechanics*, **67**, (2000), pp. 444–452. https://doi.org/10.1115/1.1311275.

[9] M. Kikuchi, Y. Wada, and Y. Li. Crack growth simulation in heterogeneous material by S-FEM and comparison with experiments. *Engineering Fracture Mechanics*, **167**, (2016), pp. 239–247. https://doi.org/10.1016/j.engfracmech.2016.03.038.

[10] A. Rajput, A. Subhash Shedbale, and D. Khan. A robust staggered localizing gradient enhanced isotropic damage model for failure prediction in heterogeneous materials. *Engineering Fracture Mechanics*, **293**, (2023), 109708. https://doi.org/10.1016/j.engfracmech.2023.109708.

[11] J. H. P. de Vree, W. A. M. Brekelmans, and M. A. J. van Gils. Comparison of nonlocal approaches in continuum damage mechanics. *Computers & Structures*, **55**, (1995), pp. 581–588. https://doi.org/10.1016/0045-7949(94)00501-s.

[12] J. Mazars, F. Hamon, and S. Grange. A new 3D damage model for concrete under monotonic, cyclic and dynamic loadings. *Materials and Structures*, **48**, (2014), pp. 3779–3793. https://doi.org/10.1617/s11527-014-0439-8.

[13] T. H. A. Nguyen, T. Q. Bui, and S. Hirose. Smoothing gradient damage model with evolving anisotropic nonlocal interactions tailored to low-order finite elements. *Computer Methods in Applied Mechanics and Engineering*, **328**, (2018), pp. 498–541. https://doi.org/10.1016/j.cma.2017.09.019.

[14] Y. Wang and H. Waisman. From diffuse damage to sharp cohesive cracks: A coupled XFEM framework for failure analysis of quasi-brittle materials. *Computer Methods in Applied Mechanics and Engineering*, **299**, (2016), pp. 57–89. https://doi.org/10.1016/j.cma.2015.10.019.

[15] T. Q. Bui and H. T. Tran. Dynamic brittle fracture with a new energy limiter-based scalar damage model. *Computational Mechanics*, **69**, (2022), pp. 1323–1346. https://doi.org/10.1007/s00466-022-02143-4.